Nuclear Instruments and Methods in Physics Research A264 (1988) 319–326
North-Holland, Amsterdam

A "DWARF BALL": DESIGN, INSTRUMENTATION, AND RESPONSE CHARACTERISTICS OF A 4π LIGHT CHARGED-PARTICLE MULTIDETECTOR SYSTEM

D.G. SARANTITES, L.G. SOBOTKA, T.M. SEMKOW, V. ABENANTE, J. ELSON, J.T. HOOD, Z. LI *, N.G. NICOLIS, D.W. STRACENER and J. VALDES

Department of Chemistry, Washington University, St. Louis, MO 63130, USA

D.C. HENSLEY

Oak Ridge National Laboratory, Oak Ridge, TN 37831, USA

Received 6 August 1987

A 4π light charged-particle spectrometer is described. The spectrometer consists of 72 fast–slow plastic scintillator phoswiches closely packed in a 4π arrangement. The device is small enough to be enclosed in the spin spectrometer scattering chamber. For each detector that fires, the fast ΔE and slow E pulse heights and a time for each group of 16 detectors are recorded. From this information protons and α particles can be identified and their energies measured over a large dynamic range. The geometry, construction, electronics and data acquisition system are discussed. Examples are given of the performance of this spectrometer from an experiment in which Si (ΔE, E) heavy-ion telescopes were used as event triggers and the spin spectrometer detected γ rays and neutrons.

1. Introduction

Reactions initiated by energetic heavy-ion beams have greatly enriched the spectrum of nuclear reactions. Between the well-known compound nucleus and direct reaction mechanisms, we now find a variety of partially equilibrated reaction mechanisms. These newly discovered processes include deeply inelastic scattering and incomplete fusion. In the study of these and other mechanisms, we find ourselves asking how the mass, the energy, and the angular momentum are distributed among the reaction products. These topics are of course related, however they are often the subject of separate experiments using different techniques.

In general, the experimental techniques employed aim to study the decay of the fragments produced in the primary process. In these reactions, the decay process is invariably complex, involving n, γ, charged particle and perhaps even fission decay. Measurements of all of these decays is often necessary in order to reconstruct the mass, energy and angular momentum of the primary fragments. We have addressed this need by constructing a 4π light charged-particle detecting device which can be used in conjunction with a 4π γ and neutron detecting device.

* Permanent address: Physics Department, Institute of Atomic Energy, Beijing, People's Republic of China.

Although emission of light charged particles is responsible for the dissipation of excitation energy from the reaction products, it removes usually a small fraction of the intrinsic angular momentum imparted to the products. Therefore, the use of a 4π γ-ray device such as the spin spectrometer [1,2] is important, since it is capable of detecting the associated γ-ray multiplicity, the total γ-ray energy, the neutron multiplicity and the neutron energy. The requirement to use the new device in conjunction with the spin spectrometer places a severe constraint on the size of the charged-particle device, in that it must fit inside the cavity of the spin spectrometer which has an inner radius of only 16 cm.

Another class of experimental investigations that a 4π charged-particle spectrometer would make possible is in-beam spectroscopic studies of high-spin nuclei that are produced in fusion reactions where many competing channels are present. Using the spin spectrometer to select the exit channel of interest by coincidence fold gating works well only for reactions where (HI, xn) are the dominant channels [3]. For neutron deficient products far from the β-stability line competing channels such as (HI, αxn), (HI, pxn), and [HI, 2p($x-1$)n], for example, cannot be distinguised by selection with γ-ray multiplicity, but they could be easily identified by selection on particle type and multiplicity with the appropriate 4π particle spectrometer. Furthermore, for reactions leading to heavy products, strong competition

from fission makes high-spin spectroscopy very difficult because 4π crystal-ball type devices cannot effectively discriminate against fission [4]. Again, a suitably designed 4π charged-particle device could very effectively discriminate against fission.

In this paper we describe the design and performance of a 4π charged-particle spectrometer built to operate in conjunction with the spin spectrometer at the Holifield Heavy-Ion Research Facility (HHIRF), at the Oak Ridge National Laboratory. We call this spectrometer the Dwarf Ball. The geometry of the Dwarf Ball is described in section 2. The electronics and data acquisition system are discussed in section 3. Finally, the performance of the plastic scintillator in measuring the α particles from the source and in-beam detection of charged particles is described in section 4.

2. Description

2.1. Geometry and construction of the Dwarf Ball

The Dwarf Ball consists of an array of up to 72 closely packed plastic–scintillator phoswiches approximating a hollow sphere with an inner radius of 43.2 mm and shell thickness of 6.25 mm. The basic geometry of the detectors and their placement in the Dwarf Ball are similar to those of the spin spectrometer [2]. Each detector is a tapered prism that can be removed radially. The cross section of twelve detectors is a regular pentagon. Each pentagonal detector is surrounded by five irregular hexagonal ones. Of the hexagons, 55 have identical shape. Five additional hexagons are placed at the forward angles and are somewhat larger in order to detect particles down to 9° from the beam. With the exception of the larger 5 forward hexagons, all other detectors subtend an equal solid angle of $4\pi/72$ sr each. As in the spin spectrometer, a pair of pentagonal detectors has been removed in order to allow for entry and exit of the beam.

The geometry of the Dwarf Ball was chosen to be identical to that of the spin spectrometer [2] for the following reasons: (a) the design features for the mechanical construction of the scintillators had already been worked out, (b) the faces of the Dwarf Ball align perfectly with the NaI detectors in the spin spectrometer and with existing access ports of the spherical scattering chamber in the spin spectrometer, (c) the number of elements (72) is sufficiently large to provide adequate angular resolution for light charged-particles from normal kinematics heavy-ion induced reactions with incident energies of $E/A \leq 12$ MeV, and (d) certain compatibility with existing software for data analysis.

A cross section through a hexagonal detector is shown in fig. 1. The thick E detectors consists of

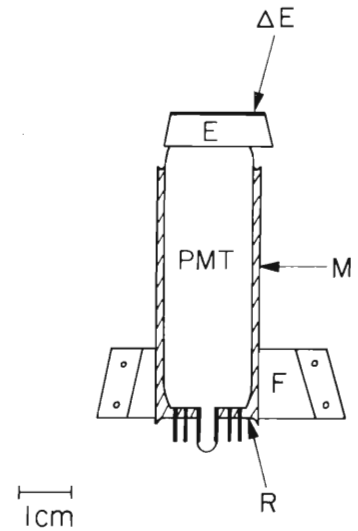

Fig. 1. A cross section through a hexagonal element of the Dwarf Ball. Abbreviations are as follows: ΔE = fast plastic, E = slow plastic, PMT = photomultiplier tube, M = μ-metal shield, R = silicone rubber, F = fin.

slow-plastic scintillator material (Bicron BC-444). They were accurately machined to their appropriate shapes and then they were optically fastened to the photomultiplier tubes. Initially this coupling was done with Bicron BC-600 optical epoxy cement. However, after our first experiment we replaced this rigid coupling with a silicon rubber compound, GE RTV-615. The thin ΔE detectors consist of fast-plastic scintillator material (Bicron BC-400). The ΔE wafers were fastened on to the E detectors with the Bicron BC-600 optical epoxy. The thickness of the optical layer was kept small (1.8 ± 0.3 mg/cm^2) by applying a pressure of 0.15 kg/cm^2 on the wafers during the curing of the epoxy. In order to eliminate optical cross talk between detectors, the sides of all the detectors were coated with TiO_2 reflector paint. The front faces were covered by a thin evaporated layer of 90 μg/cm^2 Al metal. To maximize packing there is no housing around the scintillators.

The Dwarf Ball is assembled via mating male and female plastic fins which are appropriately attached to the μ-metal shields (0.25 mm thick). The fins come together and align two sets of holes which allow pins to be inserted and provide the connecting links to a rigid superstructure. The photomultiplier tubes (PMT) were potted into the μ-metal shield with GE RTV-627 silicon–rubber compound. Each pentagonal detector assembly has 5 male fins. Each hexagonal detector assembly has one pentagon-mating female fin, one hexagon-mating male fin, and one hexagon-mating female fin.

A photograph of the Dwarf Ball is shown in fig. 2. A gyroscopic structure supports the ball and allows its alignment with the beam axis. Two opposite pentagonal

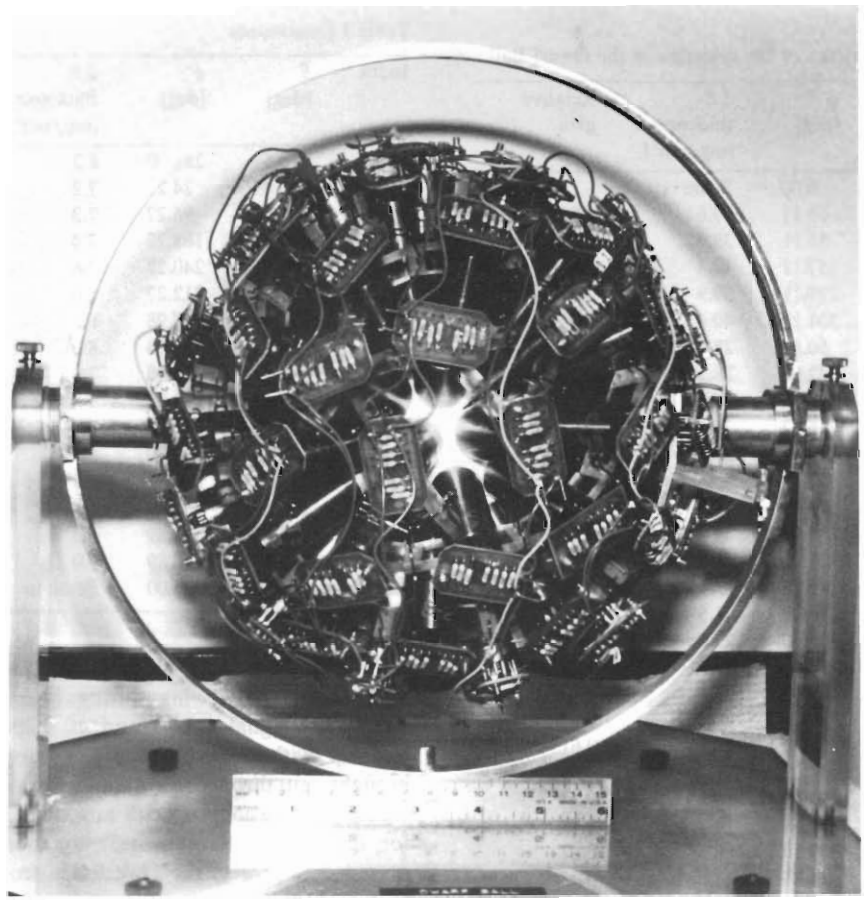

Fig. 2. Photograph of the Dwarf Ball with the photomultiplier tubes and voltages dividers attached.

detectors have been replaced by two small entrance and exit tubes that have pentagonal fins attached to them which connect to five neighbouring hexagonal detectors. An aluminum ring supports the entrance and exit tubes and transfers the support to the scattering chamber.

The angular positions of the detectors in the spectrometer are listed in table 1. The first three columns in table 1 give the index and the angles θ and ϕ. The θ and ϕ are the polar and azimuthal angles in a spherical polar coordinate system for which the outgoing beam defines the polar axis and the upward vertical direction is taken as $\phi = 0°$. The angles in table 1 correspond to the centroids of the detectors. Column 4 gives the thickness of the ΔE detectors in mg/cm^2 and the last column gives the gains of various PMTs relative to detector no. 2 measured with an α source using the slow E detectors. The detectors have been arranged in the spectrometer so that the ΔE thickness decreases with θ in order to compensate to some extent for the kinematical decrease of the particle energies at backward angles. The PMTs have been arranged so that detectors of the same θ have approximately the same gain to allow running the PMTs in groups with the same high voltage.

2.2. Reaction chamber

The reaction chamber used to house the Dwarf Ball is the standard spherical scattering chamber of the spin spectrometer (3 mm thick, 32 cm diameter) [2]. Two of the four access ports of the chamber are utilized to insert the target and to view the phosphor at the target position during focussing of the beam. Thus, in addition to the two pentagonal detectors at the beam entrance and exit, the detector no. 35 (table 1) is removed to allow entry of the target holding rod and frame. The target holder penetrates radially and it can travel a distance of ± 1.0 cm to allow exposing different target foils to the beam or to expose fresh target material to the beam for minimizing interference from carbon deposits during long bombardments. Detector no. 65 is normally removed during the focussing of the beam to allow viewing of the phosphor. An externally controlled

Table 1
Angles and characteristics of the detectors in the Dwarf Ball

Index	θ [deg]	ϕ [deg]	ΔE thickness [mg/cm^2]	Relative gain
01	0.00	0.00	Beam out	–
02	24.42	13.11	39.6	1.00
03	24.42	85.11	39.6	1.08
04	24.42	157.11	40.3	0.91
05	24.42	229.11	39.9	0.87
06	24.42	301.11	40.4	1.02
07	41.59	50.02	28.0	0.31
08	41.59	122.02	28.3	0.33
09	41.59	194.02	26.2	0.40
10	41.59	266.02	26.6	0.40
11	41.59	338.02	25.5	0.44
12	49.51	11.73	22.4	0.45
13	49.51	83.73	25.0	0.50
14	49.51	155.73	23.5	0.57
15	49.51	227.73	22.4	0.58
16	49.51	299.73	23.9	0.55
17	63.43	36.00	21.5	0.61
18	63.43	108.00	21.0	0.69
19	63.43	180.00	20.9	0.78
20	63.43	252.00	21.8	0.89
21	63.43	324.00	20.4	0.92
22	67.93	62.39	20.9	0.61
23	67.93	134.39	19.4	0.60
24	67.93	206.39	18.9	0.64
25	67.93	278.39	16.1	0.65
26	67.93	350.39	18.5	0.67
27	77.52	14.74	17.6	0.72
28	77.52	86.74	17.0	0.72
29	77.52	158.74	16.6	0.74
30	77.52	230.74	16.3	0.78
31	77.52	302.74	15.4	0.79
32	87.30	41.39	15.2	0.80
33	87.30	113.39	14.7	0.84
34	87.30	185.39	16.1	0.84
35	87.30	257.39	Target	–
36	87.30	329.39	14.5	0.91
37	92.70	66.61	10.5	0.94
38	92.70	138.61	14.0	0.97
39	92.70	210.61	12.8	1.00
40	92.70	282.61	13.0	1.01
41	92.70	354.61	11.9	1.02
42	102.48	21.26	11.6	1.04
43	102.48	93.26	11.4	1.07
44	102.48	165.26	11.3	1.07
45	102.48	237.26	10.9	1.09
46	102.48	309.26	10.7	1.11
47	112.07	45.61	10.6	1.12
48	112.07	117.61	9.2	1.15
49	112.07	189.61	9.2	1.21
50	112.07	261.61	9.0	1.23
51	112.07	333.61	9.0	1.25
52	116.57	0.00	8.6	0.96
53	116.57	72.00	8.5	1.29
54	116.57	144.00	8.4	1.32
55	116.57	216.00	8.3	1.41
56	116.57	288.00	8.2	1.83
57	130.49	24.27	7.2	1.25
58	130.49	96.27	7.3	1.27
59	130.49	168.27	7.4	1.30
60	130.49	240.27	7.6	1.34
61	130.49	312.27	8.0	1.35
62	138.41	57.98	6.6	1.35
63	138.41	129.98	8.0	1.48
64	138.41	201.98	7.0	1.50
65	138.41	273.98	Viewer	–
66	138.41	345.98	7.1	1.51
67	155.58	22.89	5.3	1.52
68	155.58	94.89	5.5	1.57
69	155.58	166.89	5.9	1.73
70	155.58	238.89	6.3	1.99
71	155.58	310.89	6.0	2.12
72	180.00	0.00	Beam in	–

light facilitates viewing during beam focussing. The coaxial 72 signal cables and 10 high voltage cables, together with those for the triggering telescopes, are brought out through an annular space within the entrance pipe. A collimator (8 mm diameter) and a shield for the plastic detector near the beam entrance are provided to protect the Dwarf Ball from stray beam or scattered particles from the entrance collimator.

2.3. Triggering of the Dwarf Ball

The present arrangement allows for a variety of triggering devices for the Dwarf Ball and/or the spin spectrometer. The Dwarf Ball can be self-triggered or can accept external triggering detectors. There is enough room between the Dwarf Ball and the walls of the spherical scattering chamber (5–7 cm) to accommodate several Si surface barrier (ΔE, E) telescopes or small gas ΔE, Si E telescopes. Small axial holes can be machined at the polyhedra vertices where 3 detectors meet in order to permit particle detection by external telescopes. If desired, individual detectors can be removed to permit larger solid angle triggering heavy-ion detectors to view the target. In order to facilitate assembly, the various triggering devices inside the scattering chamber can be attached to the superstructure of the Dwarf Ball. In an experiment described in section 4, three Si (ΔE, E) telescopes triggered the Dwarf Ball. These were attached to the Dwarf Ball superstructure and cooled to $\sim 5\,^{\circ}$C with circulating ethylene glycol. The cooling is required because the Dwarf Ball normally operates at $\sim 40\,^{\circ}$C. Other detector assemblies external to the scattering chamber can also be used to

trigger the Dwarf Ball. Among such devices are Compton-suppressed Ge detectors.

3. Electronics and data acquisition

Each phoswich consists of a 6.35 mm thick slow-plastic scintillator (Bicron BC-444) with typical 10 ns rise time (10% to 90%) and a 450 ns decay time and a variable thickness thin fast-plastic scintillator (Bicron BC-400) with 3 ns rise time and ~ 12 ns decay time. The thick E detector is coupled directly to a Hamamatsu R1666 six stage photomultiplier tube (typical gain: 10^5). The voltage divider circuit is shown in fig. 3. Each divider chain was built on a printed-circuit board with dimensions 2×3 cm^2. Each divider draws a current of 0.110 mA for an applied voltage of 1000 V. This corresponds to a total power dissipation of 7.5 W for 68 detectors. The choice of this high resistance base was dictated by the requirement to reduce the need for power as much as possible without affecting the performance of the detectors.

A schematic diagram for the electronics controlling the Dwarf Ball during an in-beam experiment is shown in fig. 4. The PMT anode signal is first amplified by a fast, variable gain (2–40) amplifier (LA). One of the

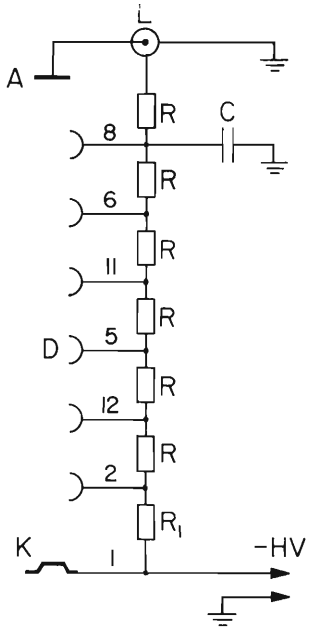

Fig. 3. Schematic diagram of the voltage divider chain built on a printed-circuit board. Abbreviations are as follows: K = photocathode, A = anode, D = dynode, R = 1.21 MΩ resistor, R_1 = 1.82 MΩ resistor, C = 0.01 μF capacitor, Lepracon connector. The numbers indicate pin positions in the socket.

two amplifier outputs is used to establish the timing of the anode pulses by means of a leading-edge discriminator. The other output of the linear amplifier is first delayed by 115 ns (RG-58 cable) and then split linearly in a ratio 4:1 for the ΔE and E analog-to-digital converters (ADC), respectively. The phoswich detectors are divided into five 16-channel groups (5th group containing several empty channels). The split linear ΔE and E signals are digitized by separate 16-channel ADC units (FERA). The timing discriminator outputs are fanned into one output for every 16 discriminator channels (OR). The event trigger is established by a logical OR of the discriminator signals from three Si telescopes.

The ADC gates for each group of 16 phoswich detectors are derived from two-fold coincidence (AND) between one of the event-trigger outputs and each 16-channel group of the Dwarf Ball discriminators. The first logical AND output is converted from NIM to ECL logic and is used to supply a prompt, 20 ns gate for the ΔE ADC. The second logical AND output is delayed 30 ns, stretched to 800 ns with a gate and delay generator (GDG), and is used to gate the E ADC. The event-trigger output also starts a set of time-to-digital converters (TDC), which are stopped by a delayed fanned output from the ΔE gate signal. This provides one TDC for each group of 16 detectors. Individual TDC channels, one for each detector, can easily be incorporated.

Fig. 4 also shows a schematic diagram of the acquisition setup for a typical in-beam experiment. Data acquisition is managed by two Event Handlers [5] which are programmable CAMAC-based microprocessors. Each of the Event Handlers controls 2 CAMAC crates containing ADC, TDC, and other modules. The Master Event Handler (MEH) provides a general control of the data acquisition. The MEH controls data from the triggering detectors (Si telescopes) and spin spectrometer (not shown in fig. 4), and provides a communication with the main computer (Perkin Elmer, PE). It also controls the Slave Event Handler (SEH), which manages the data from the Dwarf Ball.

The internal communication is established as follows. The event-trigger pulse strobes the STROBE module [5], which generates an EVENT pulse to the MEH. During an event processing the STROBE vetoes any gates from pileup events. The MEH sends the EVENT pulse to the SEH and a BUSY signal to the STROBE. After the ADC and TDC conversion the MEH reads the digitized signals from the Si telescopes and spin spectrometer and sends them to the PE computer through a transmitter (XMIT) and the system crate. The SEH reads the digitized signals from the DWARF Ball and sends them to the FIFO memory (FIFO MEM) through XMIT and receiver (REC). The MEH waits until the input BUSY and EMPTY signals disappear,

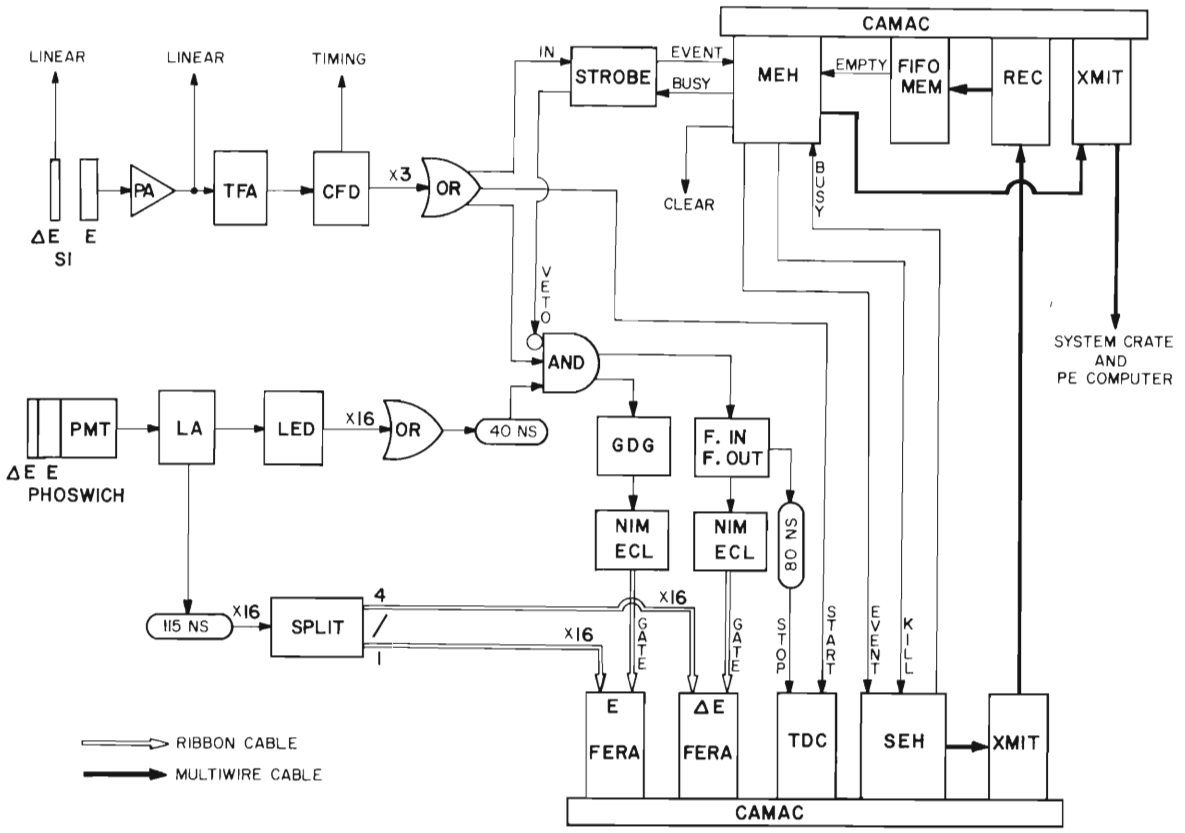

Fig. 4. Schematic diagram of the Dwarf Ball electronics and the data acquisition system. The setup shown here is for three Si telescopes and one group of 16 phoswiches. A detailed description is given in section 3. A key to the figure: PA = preamplifier (Canberra 2004); TFA = timing filter amplifier (Ortec 474); CFD = quad constant fraction discriminator (Ortec 934); OR, F.IN F.OUT = logic fan-in/fan-out (LeCroy 429A); AND = quad 2-fold coincidence unit (LeCroy 622); PMT = photomultiplier tube; LA = 6-channel variable-gain linear amplifier (LeCroy 612M); LED = leading-edge octal discriminator (LeCroy 623); GDG = gate and delay generator (ESN = GG8000); NIM ECL = ECL–NIM–ECL converter (LeCroy 4616); FERA = 16-channel analog-to-digital converter (LeCroy 4300B); TDC = octal time-to-digital converter (LeCroy 2228A); MEH = Master Event Handler; SEH = Slave Event Handler; REC = receiver; XMIT = transmitter; PE = Perkin Elmer; FIFO MEM = FIFO memory (Kinetics Systems 3841).

reads the FIFO through the CAMAC dataway and sends the data to the PE computer. The MEH has an option of rejecting the event (KILL), if it is found to be unsatisfactory. After the end of event processing the MEH sends a clear pulse to all the modules. On-line histogramming and writing on magnetic tapes is done by the PE computer.

4. Performance of the phoswich detectors

The stability with counting rate was studied separately for the fast and the slow scintillators using a collimated ^{249}Cf α source. In order to change the counting rate the ^{249}Cf source was moved radially. The 5.8 MeV α-peak position was determined using the charge integrating FERA ADC gated appropriately for the fast scintillator which was attached in front of the slow E detectors. The α particles from the ^{249}Cf stopped in all the ΔE detectors. For the stability test of the slow E detector, the ΔE wafer was removed and the α-peak position was again determined with the FERA ADC gated with a 1000 ns gate. In all these measurements the threshold was placed at $\sim 1/20$ of the α peak.

In fig. 5 we show the percent shift in the position of the α peak for fast plastic as a function of the counting rate at four applied high voltages of 700, 900, 1100 and 1300 V. It is seen that the peak position moves down as the counting rate increases and the percent gain shift increases as the applied voltage is increased. Good stability is seen for voltages below about 900 V. The stability for the slow plastic with counting rate and applied voltage behaves quite differently as can be seen from fig. 6. Here for lower applied voltage, the peak position moves to larger pulse heights as the counting

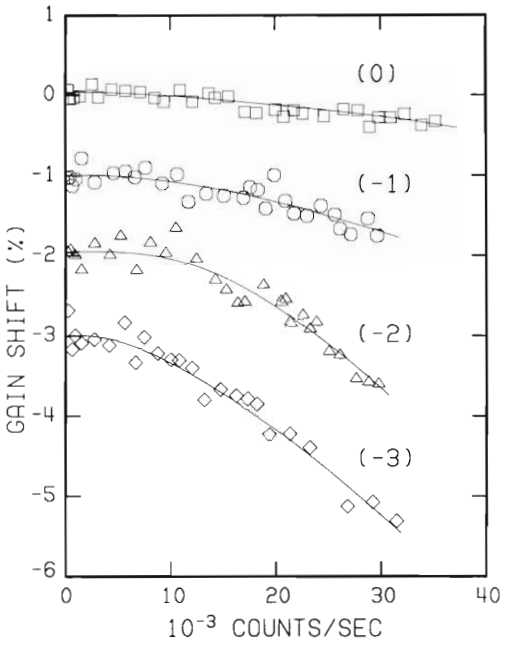

Fig. 5. Shift (%) of the 5.8 MeV α-peak position from a ^{249}Cf source as a function of counting rate measured at different operating voltages for the fast plastic ΔE scintillators. Abbreviations are as follows: □ = 700 V (0%), ○ = 900 V (−1%), △ = 1100 V (−2%), and ◇ = 1300 V (−3%). The points were graphically shifted on the Y axis by the values given in parentheses above in order to better illustrate the trends. The lines have been drawn to guide the eye.

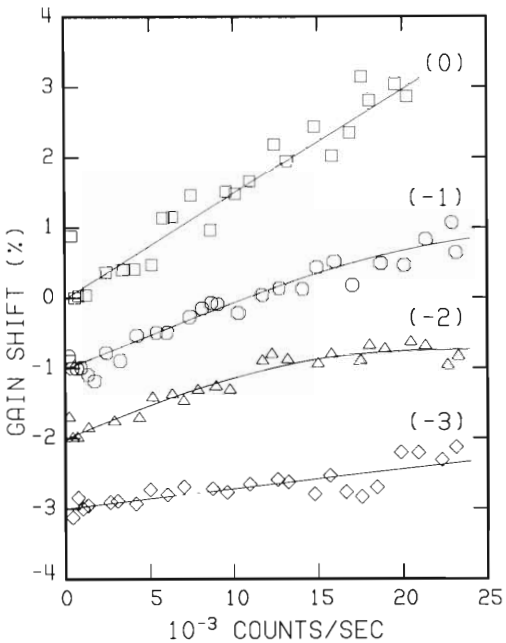

Fig. 6. Same as fig. 5 for slow plastic E scintillators.

rate increases. For the highest measured voltage of 1300 V the peak stability with counting rate improves considerably. The gain shift is determined primarily by two factors. On the one hand, we have the load on the PMT tube with increasing voltage and, on the other hand, there is the effect of pulse pileup. For the fast scintillator, with the narrow gate, the gain shift is determined by the load on the PMT (fig. 5). For the slow scintillator, with the wide gate, the pileup dominates at low voltages. As the voltage is increased, the load on the PMT pulls the output down and causes the levelling off of the gain shift with counting rate (fig. 6).

The energy resolution of the plastic scintillators was studied with the ^{249} Cf α source and with 22 MeV protons from tandem accelerator at HHIRF. The peak width for 5.8 MeV α particles in fast plastic had a fwhm of 13% at a low counting rate, which increased to 15% at the high counting rate. The distributions from the slow plastic had fwhm values of 18% which did not depend on the counting rate. In the case of protons we used (p, p′) scattering on ^{12}C and ^{16}O. The resolution was determined only for slow plastic, since the protons lose a very small fraction of their energy in the fast plastic. The typical fwhm of proton elastic-scattering and inelastic-scattering (4.4 MeV ^{12}C and 6.1 MeV ^{16}O) peaks was (17 ± 6)% for most of the detectors.

The Dwarf Ball was used in an experiment at HHIRF aimed at studying the excitation energy distribution in binary reactions. We used the 11.9 MeV/nucleon ^{28}Si + ^{181}Ta reaction. Projectile-like fragments were detected in three Si telescopes, which served as event triggers. The Dwarf Ball detected the light charged particles, and the spin spectrometer was used to detect γ rays and the neutrons.

A directly measured (ΔE, E) map for a Dwarf Ball detector centered at $\theta = 49.5°$ is shown in fig. 7a. The map shows that protons and α particles are well separated. Low energy electrons, protons, α particles, and heavy ions stop completely in the ΔE detector and form a line close to the ΔE axis (called s_1 line). Some γ rays were detected in addition to protons and α particles. They form the s_2 line seen in fig. 7a. An intense peak near the origin corresponds to low energy electrons, X rays and the pedestal. Due to the prompt rise and exponential decay of the fast- and slow-plastic signals as well as finite widths of the fast (20 ns) and slow (800 ns) gates, there is some mixing of the fast and slow signals. In other words the ΔE signal will contain some of the slow component and the E signal will contain some of the fast component. The amount of this mixing is proportional to the slopes of s_1 and s_2 lines in fig. 7a. If there were no mixing, the particles stopping in the ΔE detector would contribute only to the ΔE gate, and the s_1 line would be on the X axis. Similarly, the γ rays interact primarily with the slow plastic (the fast plastic is very thin), and the s_2 line would be on the Y axis, if

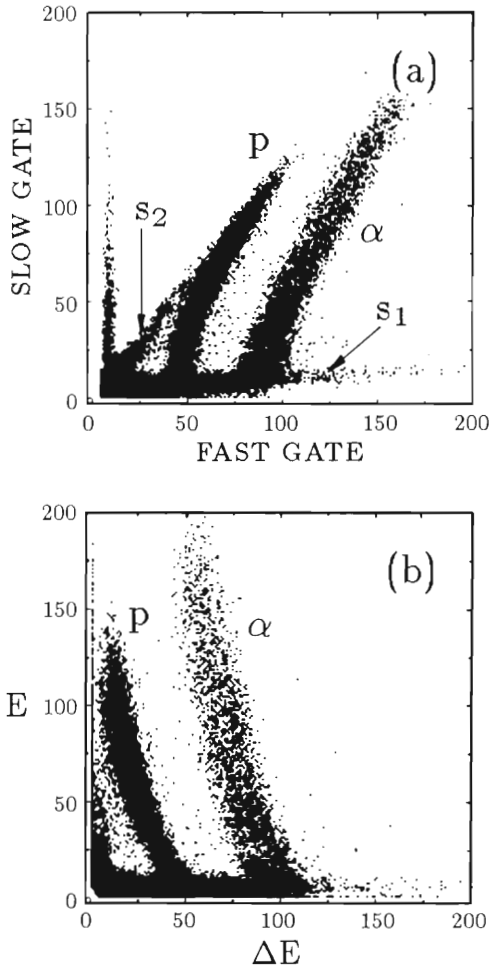

Fig. 7. (a) Plot of the integrated charge with the fast gate vs, the slow gate for one of the Dwarf Ball detectors centered at $\theta = 49.5°$. The map shows proton and α particles detected in the reaction 11.9 MeV nucleon $^{28}Si + ^{181}Ta$. (b) ΔE vs E map of the data from (a) after correction for the mixing of the fast and slow signal components. The X and Y axes on both figures are in arbitrary units.

there were no mixing. The mixing can be removed using the following relations:

$$x' = \frac{x_2(1 + Rs_1)}{s_2 - s_1}\left(x - \frac{1}{s_2}y\right),$$

$$y' = \frac{1/R + s_2}{s_2 - s_1}(y - s_1 x),$$

where R is the signal splitting ratio between the fast and the slow gates (typically ~ 4); s_1, s_2 are the slopes of the s_1, s_2 lines; x, y are the original ΔE and E channels; x', y' are the ΔE and E channels after correction. By applying this procedure event-by-event one obtains a corrected (ΔE, E) map shown in fig. 7b. This correction has been found to be useful for calibration purposes as well as in deducing ΔE energy losses from residual energy measurements and calculations.

In summary, we have designed and constructed a small 4π light charged-particle multidetector system which can be operated in conjunction with the spin spectrometer, a 4π γ-ray multidetector spectrometer. This device enables more comprehensive and exclusive studies of reaction mechanisms and nuclear spectroscopy at high spins.

Acknowledgements

The excellent cooperation and the fine craftmanship of the staff of the Department of Chemistry Machine Shop at Washington University during the construction of the Dwarf Ball is greatly appreciated. This work was supported in part by the US Department of Energy under contract nos. DE-AS02-76ER04052 and DE-AC02-85ER40210. One of us (L.G.S.) acknowledges support from a US Presidential Young Investigator award. Oak Ridge National Laboratory is operated by Martin Marietta Energy Systems, Inc., under contrast no. DE-AC-84OR21400 with the US Department of Energy.

References

[1] D.G. Sarantites, R. Lovett and R. Woodward, Nucl. Instr. and Meth. 171 (1980) 503.
[2] M. Jääskeläinen, D.G. Sarantites, R. Woodward, F.A. Dilmanian, J.T. Hood, R. Jääskeläinen, D.C. Hensley, M.L. Halbert and J.H. Barker, Nucl. Instr. and Meth. 204 (1983) 385.
[3] D.G. Sarantites, M. Jääskeläinen, R. Woodward, F.A. Dilmanian, D.C. Hensley, J.H. Barker, J.R. Beene, M.L. Halbert and W.T. Milner, Phys. Lett. 115B (1982) 441.
[4] D.G. Sarantites et al., in: High Angular Momentum Properties of Nuclei, ed., N.R. Johnson (Harwood, New York, 1983), p. 417.
[5] A larger version of the device described by D.C. Hensley, IEEE Trans. Nucl. Sci. NS-26 (1979) 4454.